

Feasibility study of the forward-backward asymmetry of the $e^+e^- \rightarrow t\bar{t}$ process in all-hadronic decay modes at $\sqrt{s} = 500$ GeV with the ILD detector

Katsumasa Ikematsu*, Akiya Miyamoto, and Keisuke Fujii

High Energy Accelerator Research Organization (KEK),
Tsukuba, 305-0801, Japan

We have studied the measurement accuracy of the forward-backward asymmetry of the $e^+e^- \rightarrow t\bar{t}$ process in the 6-jet mode at $\sqrt{s} = 500$ GeV with the ILD detector. In the analysis the vertex charges of b -jets were used to distinguish t from \bar{t} in each event. The distribution of the cosine of the reconstructed polar angle of so identified t or \bar{t} showed a clear forward-backward asymmetry. After the correction for charge misidentification the forward-backward asymmetry was determined to be $A_{FB}^t = 0.334 \pm 0.0079$ for 500 fb^{-1} with the beam polarization combination of $P(e^+, e^-) = (+30\%, -80\%)$, demonstrating a very good statistical accuracy ($\sim 2\%$) even in the 6-jet mode.

1 Introduction

The forward-backward asymmetry of the $e^+e^- \rightarrow t\bar{t}$ process is sensitive to the $t\bar{t}Z$ and $t\bar{t}\gamma$ couplings and serves as a probe for new physics, which may appear as anomaly in these couplings.

Needless to say we have to distinguish t from \bar{t} in each event in order to measure the forward-backward asymmetry, A_{FB}^t . In the lepton+4-jet mode, it is straightforward because the lepton charge tells the charge of the leptonically decayed W , and hence identifies its parent to be either t or \bar{t} . In the 6-jet mode, however, we need some other way to separate t and \bar{t} , which is non-trivial. Nevertheless it is worth investigating the feasibility of A_{FB}^t measurement in the 6-jet mode, since it has a major branching fraction of 46%. In addition, the kinematical fit works better in the 6-jet mode than in the lepton+4-jet mode, where a large energy is taken away by the neutrino from the leptonically decayed W . The 6-jet mode might, hence, be advantageous when the influence of beamstrahlung is significant.

In this paper, we use the vertex charges of b jets to distinguish t from \bar{t} in each event. The measurement of the vertex charges requires a high performance detector system as well as a sophisticated reconstruction algorithm. The forward-backward asymmetry in the 6-jet mode is therefore a very good measure for the overall performance of a detector system, hence being included as one of the ILC LoI benchmarks [1]. The benchmark conditions are the center of mass energy of $\sqrt{s} = 500$ GeV, an integrated luminosity of 500 fb^{-1} , and a beam polarization combination of $P(e^+, e^-) = (+30\%, -80\%)$.

The ILD [2] is equipped with an unprecedentedly excellent vertex detector, which allows efficient b -jet charge identification with the vertex charge. The vertex charges of b jets were reconstructed by the LCFIVertex algorithm [3].

This paper is organized as follows. After we briefly describe our analysis framework in section 2, we move on to the vertex charge reconstruction and show how well we can identify

*Corresponding author. e-mail address: Katsumasa.Ikematsu@kek.jp

each jet as b or \bar{b} in section 3. We then apply this to t/\bar{t} identification for the determination of the production angle distribution ($dN/d\cos\theta_t$) in section 4. After the correction for charge misidentification we derive the A_{FB}^t and discuss the result in comparison with the Monte Carlo truth in section 5. Section 6 summarizes our analysis and concludes this paper.

2 Analysis framework

In general, Monte Carlo (MC) simulation consists of the following steps: event generation, detector simulation, event reconstruction, and data analysis.

All of the MC event samples, both the signal and the backgrounds, used in this study were produced in the StdHep [5] format by a SLAC team [4] as common inputs to LoI studies, using WHIZARD 1.4 [6] for generating parton 4-momenta and PYTHIA 6.2 [7] for parton-showering and hadronization. The beam energy spread and the beamstrahlung were properly taken into account using the spectrum generated with Guinea-Pig [8] for the default ILC design parameters at $\sqrt{s} = 500$ GeV.

The final-state particles output in the StdHep format from the event generation step were passed to a Geant4-based detector simulator called Mokka [9] and swum through the ILD detector to create exact hits in trackers and calorimeters.

These exact hits were smeared or digitized, if necessary, depending on the detector elements in the first part of MarlinReco [10] [11]. The pattern recognition was done for the smeared tracker hits, separately in the TPC and the silicon detectors and so found track segments were then linked together and fed into a Kalman-filter-based track fitter in the second part of MarlinReco. From the fitted tracks and the calorimeter hits, individual particles were reconstructed as particle flow objects (PFO) with a sophisticated particle flow algorithm called PandoraPFA [12] in the third part of MarlinReco.

These PFOs were forced to cluster into 6 jets for the signal and all background events with Durham jet clustering algorithm [13] in the fourth part of MarlinReco.

The next step is heavy flavour tagging with LCFIVertex [3]. The LCFIVertex package consists of two parts. The first part is to search for secondary and tertiary vertices inside each jet and locate them, thereby determining the decay length, the transverse mass, and the momentum at each of these vertices. In the second part these quantities are translated into the impact parameter joint probability and the highest two impact parameter significances, which are used as inputs into a neural net (NN) trained with jet samples having 0 and 1 or more secondary vertices. Each reconstructed jet is then assigned with the three NN outputs, corresponding to b -, c -, and bc -tags.

Once a bottom-flavoured jet is identified we can determine whether it is b or \bar{b} by measuring the vertex charge. We will discuss this in detail in section 3.

The reconstruction of $e^+e^- \rightarrow t\bar{t}$ events in 6-jet final states has been studied extensively in the context of the top quark mass measurement. The top quark mass in the 6-jet mode is one of the benchmark observables for ILC LoIs and the ILD study has been reported in reference [2]. Similar to the top quark mass measurement, the measurement of the forward-backward asymmetry requires a correct jet-parton association. In this paper we employed the same reconstruction algorithm as those used for the top quark mass measurement. For the reconstruction, therefore, we refer the readers to the above reference.

3 Vertex charge reconstruction and its performance for a single b -jet

In principle, we can tell which three jets are from top and the rest from anti-top in the 6-jet final state by identifying either a b/\bar{b} -jet or a c/\bar{c} -jet from W^+/W^- decay as shown in Fig. 1. In this analysis, however, we used only b/\bar{b} -jets for the top/anti-top separation.

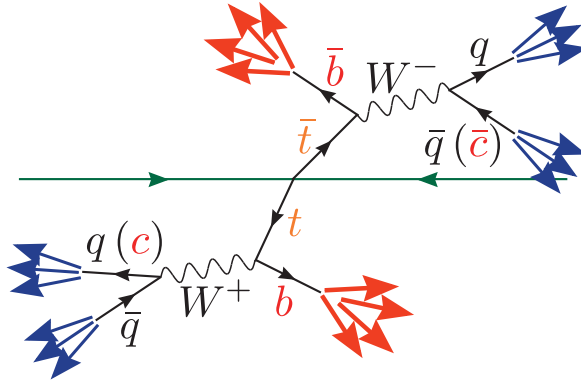


Figure 1: Schematic diagram showing fully hadronic decay channel of $e^+e^- \rightarrow t\bar{t}$ process

A bottom quark hadronizes into a B -hadron, which flies over a finite distance thanks to its large $c\tau$, making a secondary vertex significantly away from the primary vertex and hence identifiable by the vertex detector. We define the vertex charge as the sum of the charges of the charged tracks associated with the secondary vertex. If the charged tracks are reconstructed and associated perfectly, the vertex charge is equal to the charge of the primary B -hadron, from which the charge sign of the b/\bar{b} is uniquely determined.

In practice, however, there is no perfect vertexing, and the resultant distribution of the vertex charges of charged B -hadrons will have a finite width and hence their charges might sometimes be mis-identified. By the same token, the charges of neutral B -hadrons might be mis-identified, causing confusion in bottom charge sign identification.

Figure 2 shows the distribution of the MC level vertex charge, which is defined by the charge of a B -meson (B^\pm or B^0) involved in the jet tagged as a b -jet.

Inspection of the figures tells us that we can separate B^+ s from B^- s by selecting jets with negative or positive vertex charges with some contamination from B^0 s.

Figure 3 shows the distribution of the reconstructed vertex charges of the jets which are b -tagged. In this distribution the b -quark (\bar{b} -quark) contribution is shown by hatched blue (red).

The charge sign identification efficiency for a single b -jet using the vertex charge is 28% with a purity of 75%. Notice that only 40% of the b -jets hadronize into charged B -hadrons and hence maximum efficiency one can hope for is 40% in this method.

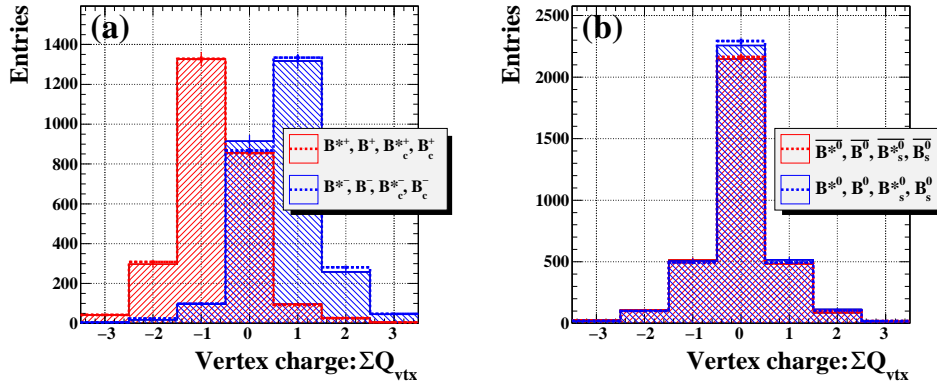


Figure 2: Reconstructed vertex charge distributions for (a) charged B -mesons and (b) neutral B -mesons as separated using MC truth information (PDG particle ID code).

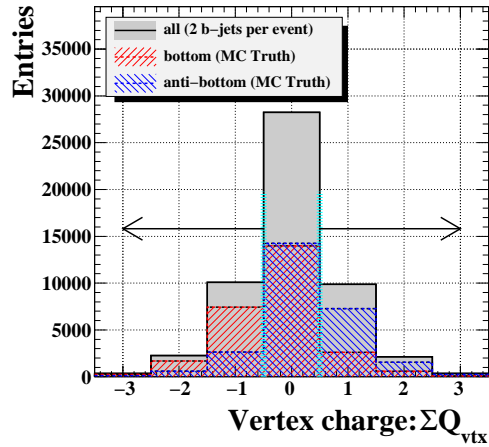


Figure 3: Reconstructed vertex charge distributions for b -quarks (hatched red) and \bar{b} -quarks (hatched blue), as identified using MC truth information, shown together with that of all the reconstructed b -jets (solid gray).

4 t and \bar{t} identification and determination of the production angle distribution ($dN/d \cos \theta_t$)

Let's call two reconstructed top systems t_1 and t_2 and b -tagged jets associated to them b_1 and b_2 , respectively. The identification of t and \bar{t} is performed by using the vertex charges of b_1 and b_2 as follows. We define c_i ($i = 1$ and 2) as the vertex charge of b_i and $C \equiv c_1 - c_2$ as the event charge. If C is 0, the event is thrown away as we cannot tell t from \bar{t} . If C is positive, t_1 is t , while if C is negative, t_1 is \bar{t} . The typical distribution of the event charge C is shown in Fig. 4.

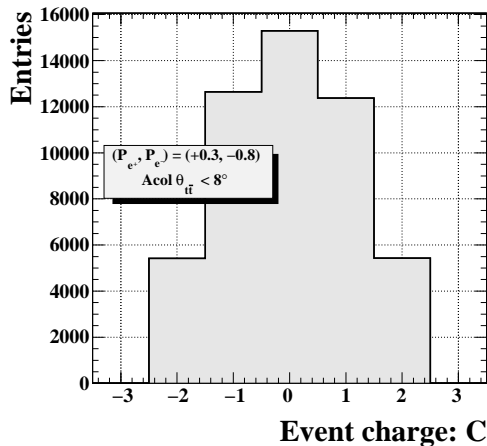


Figure 4: Distribution of event charge: $C = c_1 - c_2$.

Figures 5-(a) through -(i) show the distributions of the production angle of t_1 for 9 possible combinations of the signs of the vertex charges: c_1 and c_2 , for the samples where both W bosons decayed into light quarks.

We can see a clear forward-backward asymmetry in the case of $C \neq 0$ (Figs. 5-(a) to -(f)). Notice also that in the first row (-(a) to -(c)) t_1 is t while in the second row (-(d) to -(f)) t_1 is \bar{t} , and hence showing opposite asymmetries. On the other hand, in the case of $C = 0$, for which the charge signs of both b -jets were undetermined or they were inconsistent (both b_1 and b_2 had the same sign), there is no forward-backward asymmetry visible. In each figure the contribution from the events with wrong charge sign is hatched red, showing an opposite forward-backward asymmetry. Hatched blue is that from the combinatorial background in which the reconstructed b -jet candidates were not actually b -jets, showing no forward-backward asymmetry.

The combinatorial background depends on the flavour into which W bosons decay. Figures 6-(a) through -(i) are the same figures as Figs. 5-(a) through -(i), but plotted for the samples where one of the two W bosons decayed into a c/\bar{c} -quark. Figures 7-(a) through -(i) are similar figures for the samples where both W bosons decayed into c/\bar{c} -quarks. We

can see clearly that the combinatorial background grows with the number of c -jets in the final states, since the probability of mis-identifying charm as bottom increases.

If C is positive, t_1 is t , while if C is negative, t_1 is \bar{t} . If we can assume that t_1 and t_2 are back-to-back, the production angle of t is obtained from the angle of t_1 as

$$\cos\theta_t \equiv \sigma_C \cdot |\cos\theta_{t_1}|, \quad (4.1)$$

where σ_C is the sign of C . In order to test this assumption we compared the distributions for t_1 with those of t_2 after reflection (hatched green) in Figs. 5, 6, and 7-(d) to -(f). This comparison confirmed the assumption*, allowing us to use Eq. (4.1) to combine all the figures with $C \neq 0$. The selection efficiency of this cut is 69%.

The differential cross section for $e^+e^- \rightarrow t\bar{t}$ and consequently its forward-backward asymmetry (A_{FB}^t) depend on the center-of-mass energy of the $t\bar{t}$ system, which, in turn, depends on the amount of initial state radiation and beamstrahlung. In order to make A_{FB}^t well-defined, we hence rejected events with \sqrt{s} significantly less than 500 GeV, by requiring the acollinearity between t_1 and t_2 to be less than 8° . This final cut discarded 24% of the events so far survived. The overall selection efficiency is 20% for fully hadronic $t\bar{t}$ events.

The resultant production angle distribution is shown in Fig. 8. Of the final sample 83% have correctly identified signs of top quark charge.

5 Determination of A_{FB}^t

The production angle distribution Fig. 8 is distorted by the charge mis-identification. The distortion can be corrected by using the following formulae:

$$\begin{cases} dN_{\text{obs}}(\theta) &= p(\theta) \cdot \eta(\theta) \cdot \mathcal{L} \cdot d\sigma(\theta) + \bar{p}(\pi - \theta) \cdot \eta(\pi - \theta) \cdot \mathcal{L} \cdot d\sigma(\pi - \theta) + dB(\theta) \\ dN_{\text{obs}}(\pi - \theta) &= p(\pi - \theta) \cdot \eta(\pi - \theta) \cdot \mathcal{L} \cdot d\sigma(\pi - \theta) + \bar{p}(\theta) \cdot \eta(\theta) \cdot \mathcal{L} \cdot d\sigma(\theta) + dB(\pi - \theta) \end{cases} \quad (5.2)$$

where $\eta(\theta)$ is the acceptance, $p(\theta)$ ($\bar{p}(\theta)$) is the probability of correctly (wrongly) assigning the charge sign at production angle θ , and \mathcal{L} is the integrated luminosity.

$p(\theta)$ and $\bar{p}(\theta)$ are plotted in Fig. 9 as the black and red lines, respectively.

The figure shows no θ -dependency, allowing us to set $p(\theta) = p$ and $\bar{p}(\theta) = \bar{p}$. Solving for $d\sigma(\theta)$, we thus obtain the following formula for the differential cross section:

$$d\sigma(\theta) = \frac{p \cdot (dN_{\text{obs}}(\theta) - dB(\theta)) - \bar{p} \cdot (dN_{\text{obs}}(\pi - \theta) - dB(\pi - \theta))}{(p^2 - \bar{p}^2)\eta(\theta) \cdot \mathcal{L}}. \quad (5.3)$$

Figure 10 shows the production angle distribution after the correction for the charge mis-identification.

The acceptance function $\eta(\theta)$ is in general θ -dependent. In our case, however, it turned out that the θ -dependence was negligible[†]. The acceptance hence cancels out in the calculation of the forward-backward asymmetry, resulting in

$$A_{FB}^t = \frac{\int_{0 < \theta < \pi/2} dN(\theta) - \int_{\pi/2 < \theta < \pi} dN(\theta)}{\int_{0 < \theta < \pi/2} dN(\theta) + \int_{\pi/2 < \theta < \pi} dN(\theta)}, \quad (5.4)$$

* Strictly speaking, Eq. (4.1) does not hold on an event-by-event basis because of initial state radiation and beamstrahlung. On average, however, t_1 and t_2 are back-to-back, allowing us to merge the six cases with $C \neq 0$.

[†] Notice that for the reconstructed t or \bar{t} , being a 3-jet system, there is no acceptance hole even at $\theta = 0$ or π .

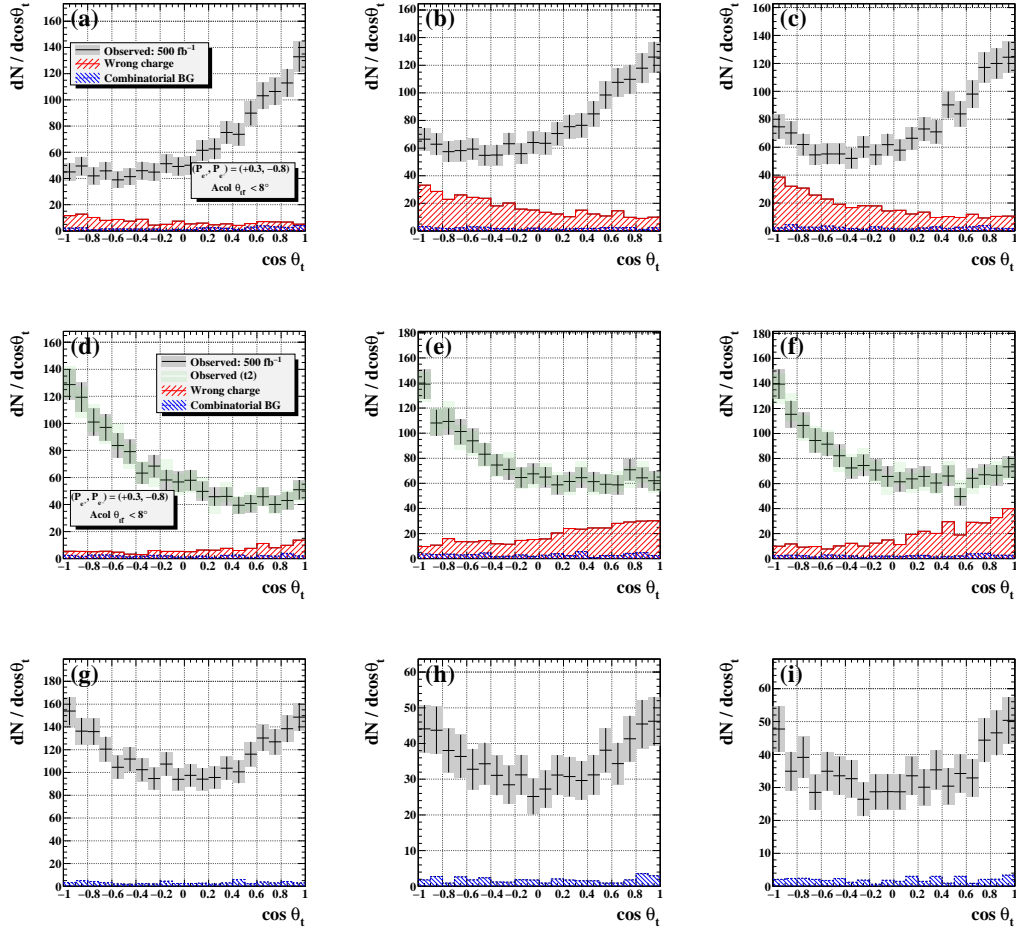


Figure 5: Distributions of the reconstructed polar angle of the identified top quark in fully-hadronic $t\bar{t}$ events, which are tagged as $(Q_{b_1}, Q_{b_2}) =$ (a) $(+, -)$, (b) $(+, 0)$, (c) $(0, -)$, (d) $(-, +)$, (e) $(-, 0)$, (f) $(0, +)$, (g) $(0, 0)$, (h) $(+, +)$, and (i) $(-, -)$ for the sample in which both W bosons decayed into light-quark pairs ($bbuddu$ sample).

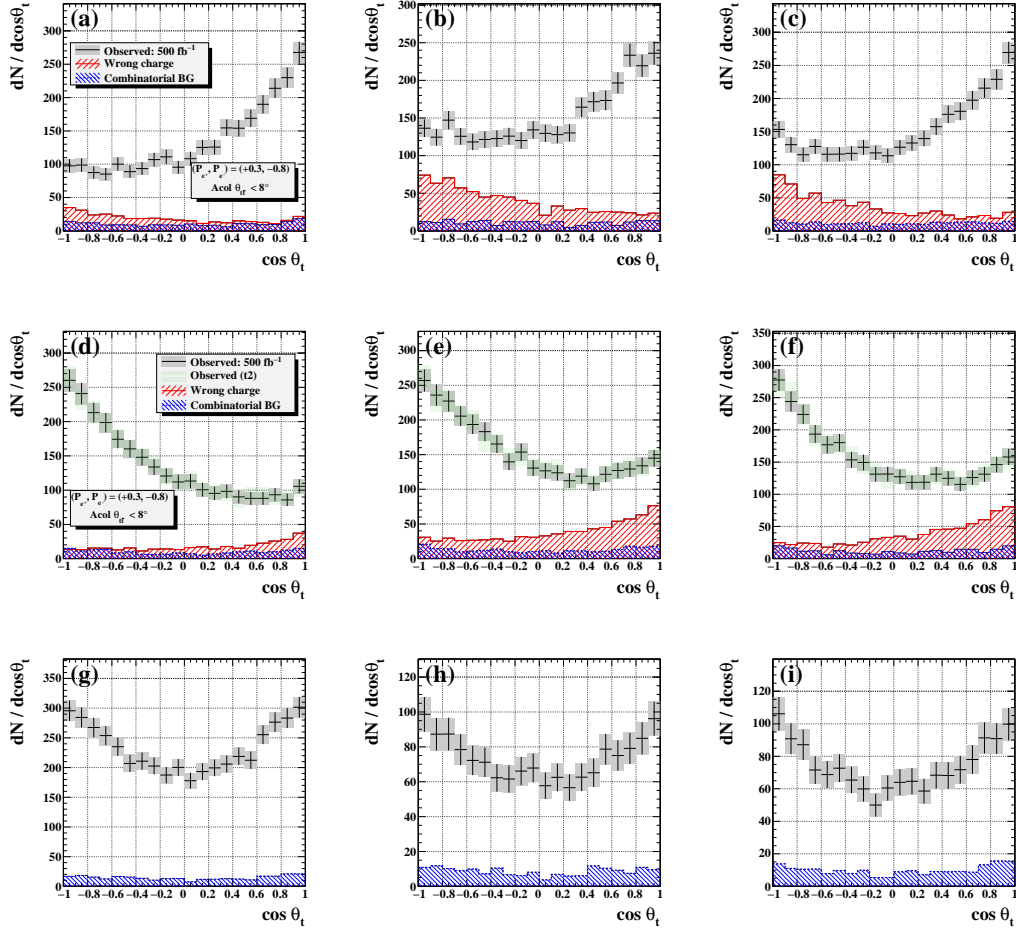


Figure 6: Distributions of the reconstructed polar angle of the identified top quark in fully-hadronic $t\bar{t}$ events, which are tagged as $(Q_{b_1}, Q_{b_2}) =$ (a) $(+, -)$, (b) $(+, 0)$, (c) $(0, -)$, (d) $(-, +)$, (e) $(-, 0)$, (f) $(0, +)$, (g) $(0, 0)$, (h) $(+, +)$, and (i) $(-, -)$ for the samples in which one of the two W bosons decayed into a c/\bar{c} -quark ($bbudsc/bbcsdu$ samples).

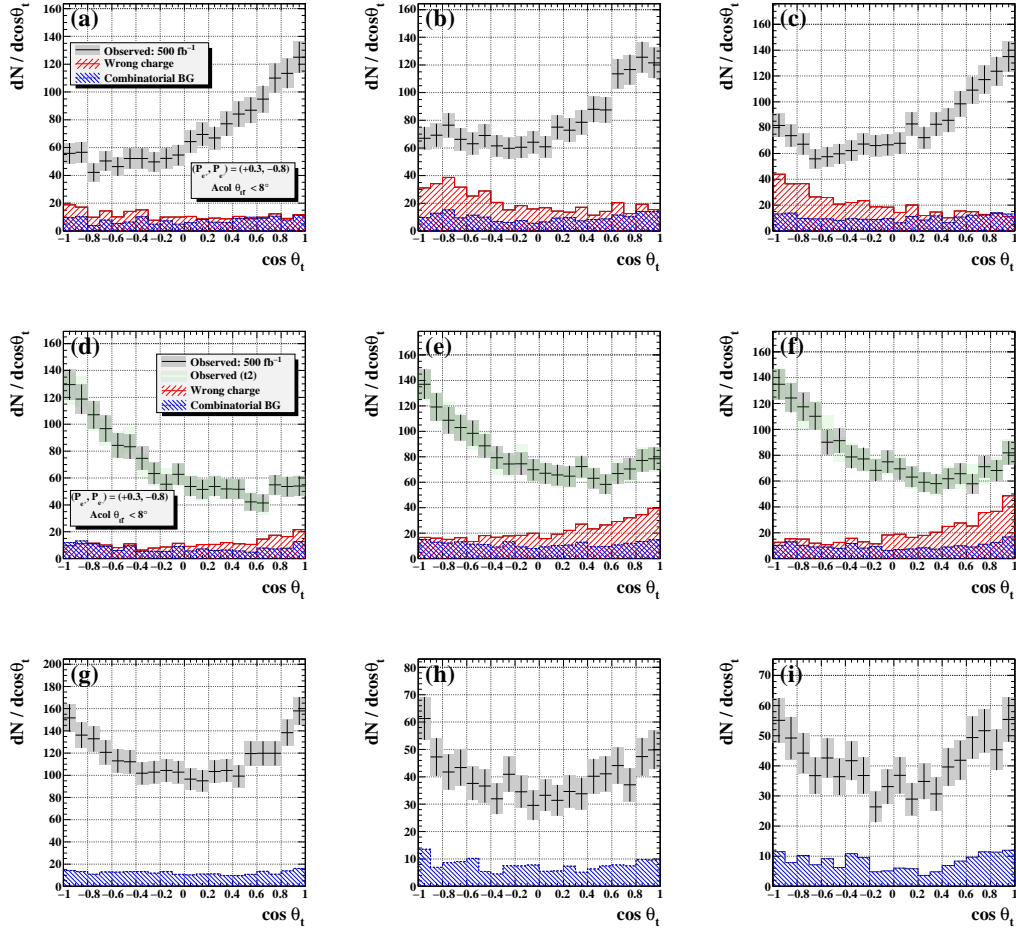


Figure 7: Distributions of the reconstructed polar angle of the identified top quark in fully-hadronic $t\bar{t}$ events, which are tagged as $(Q_{b_1}, Q_{b_2}) =$ (a) $(+, -)$, (b) $(+, 0)$, (c) $(0, -)$, (d) $(-, +)$, (e) $(-, 0)$, (f) $(0, +)$, (g) $(0, 0)$, (h) $(+, +)$, and (i) $(-, -)$ for the sample in which both W bosons decayed into c/\bar{c} -quarks ($bb\bar{c}ss\bar{c}$ sample).

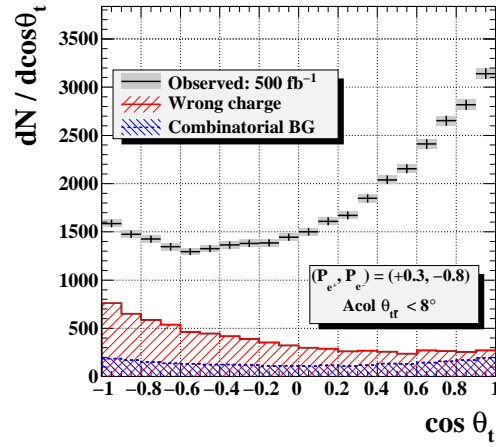


Figure 8: Distribution of the reconstructed polar angle of the identified top quark in fully-hadronic $t\bar{t}$ events. The contributions from events with the wrong charge (red) and the case where the b -quark is mis-identified are also shown (blue).

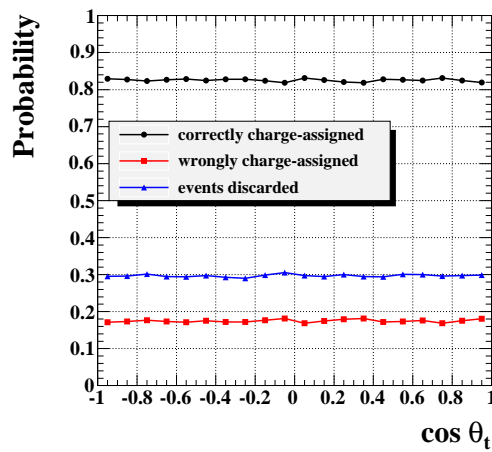


Figure 9: $\cos\theta_{t1}$ dependence of the charge-sign identification (black) and mis-identification (red) probabilities.

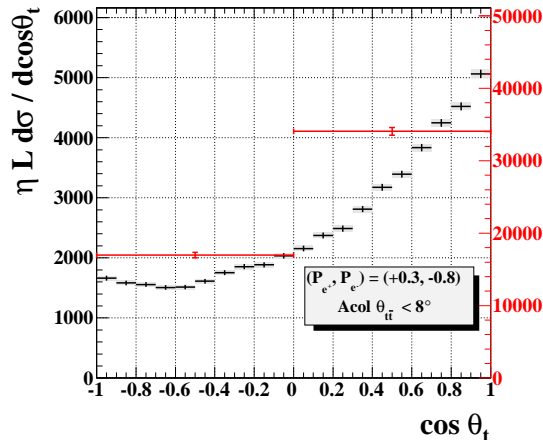


Figure 10: $\cos \theta_{t1}$ distribution after the correction for the charge mis-identification.

where $dN(\theta) \equiv \eta \cdot \mathcal{L} \cdot d\sigma(\theta)$.

From Fig. 10 we finally obtain

$$A_{FB}^t = 0.334 \pm 0.0079 \text{ (stat.)}, \quad (5.5)$$

where the center of mass energy of $\sqrt{s} = 500$ GeV, an integrated luminosity of 500 fb^{-1} , and a beam polarization combination of $P(e^+, e^-) = (+30\%, -80\%)$.

6 Summary

We have studied the measurement accuracy of the forward-backward asymmetry with the ILD detector for the $e^+e^- \rightarrow t\bar{t}$ process in the 6-jet mode at $\sqrt{s} = 500$ GeV. In the analysis the vertex charges of b -jets were used to identify t and \bar{t} . The efficiency to tag the vertex charge of a b -jet was 28% with the purity of 75%. Having two b -jets in each event, the probability to identify t and \bar{t} in the event was 71% with the probability of wrong charge assignment of 12%. The measured angular distribution was corrected for wrong t/\bar{t} charge assignments. From the number of events in forward and backward hemispheres after the correction, we obtained $A_{FB}^t = 0.334 \pm 0.0079$, where quoted error is statistical only.

Acknowledgments

The authors wish to thank all the members of the ILD optimization group for useful discussions and comments. This study is supported in part by the Creative Scientific Research Grant No. 18GS0202 of the Japan Society for Promotion of Science (JSPS) and the JSPS Core University Program.

References

- [1] “Benchmark Reactions for the ILC LOI process”, The WWSOC Software panel, http://ilcdoc.linearcollider.org/record/14681/files/Benchmark_Reactions_for_the_ILC_LOI.pdf
- [2] The ILD Letter of Intent, <http://www.ilcld.org/documents/ild-letter-of-intent/>
- [3] D. Bailey *et al.* [LCFI Collaboration], Nucl. Instrum. Meth. A **610**, 573 (2009) [arXiv:0908.3019 [physics.ins-det]].
- [4] Standard Model Data Samples, <https://confluence.slac.stanford.edu/display/ilc/Standard+Model+Data+Samples>
- [5] StdHep, <http://cepa.fnal.gov/psm/stdhep/>
- [6] W. Kilian, T. Ohl, and J. Reuter, “WHIZARD: Simulating Multi-Particle Processes at LHC and ILC” [arXiv: 0708.4233 [hep-ph]].
- [7] T. Sjostrand, L. Lonnblad, and S. Mrenna, “PYTHIA 6.2: Physics and manual” [arXiv:hep-ph/0108264].
- [8] D. Schulte, Ph. D. Thesis, University of Hamburg 1996 [TESLA-97-08].
D. Schulte, M. Alabau, P. Bambade, O. Dadoun, G. Le Meur, C. Rimbault and F. Touze, *In the Proceedings of Particle Accelerator Conference (PAC 07), Albuquerque, New Mexico, 25-29 Jun 2007, pp 2728.*
- [9] P. Mora de Freitas and H. Videau, [LC-TOOL-2003-010].
- [10] F. Gaede, Nucl. Instrum. Meth. A **559**, 177 (2006).
- [11] O. Wendt, F. Gaede and T. Kramer, Pramana **69**, 1109 (2007) [arXiv:physics/0702171].
- [12] M. A. Thomson, Nucl. Instrum. Meth. A **611**, 25 (2009) [arXiv:0907.3577 [physics.ins-det]].
- [13] Yu. L. Dokshitzer. *J. Phys. G* **17**, 1537 (1991).